

A High Rate Pixelated Neutron Detector for Neutron Reflectometry Instruments at the Spallation Neutron Source

Su-Ann Chong

Ph.D. Defense

University of Tennessee, Knoxville
Nuclear Engineering Department

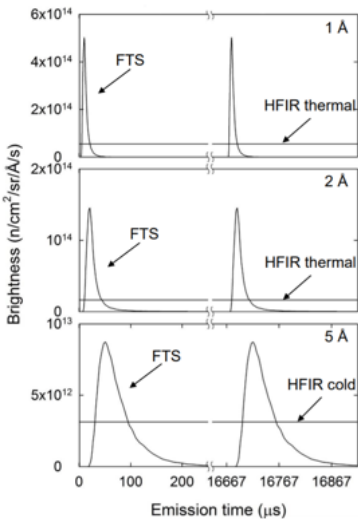
March 23rd, 2022

Outline

- ① Introduction
- ② Detector Design and Construction
- ③ Detector Characterization
- ④ Reflectivity Experiment
- ⑤ Conclusion

Spallation Neutron Source (SNS)

- The SNS a 1.4 MW accelerator-based neutron source facility that delivers short intense neutron pulses at 60 Hz.
- It is a user facility that enables researchers to conduct scientific research using neutron scattering techniques.
- Neutron sources for neutron scattering experiments are typically based on one of the two principles: fission and spallation [17].
- The distinction in neutron beam profile between a reactor and a spallation source is important to address for the detector rate requirement for different neutron sources.



HFIR stands for the High Flux Isotope Reactor (reactor) and FTS stands for the First Target Station (spallation source).

Advantages of Neutron Scattering

- **Transparency** Neutrons have zero electric charge and electric dipoles. They can penetrate materials deeply without Coulomb scattering [3, 17].
- **Magnetism** Neutrons have a non-zero magnetic moment, which can couple directly to spatial and temporal variation of material magnetization on atomic scale.
- **Isotopes and light elements** Neutron scattering length, b varies wildly with the atomic number and mass number.
- **Energy and wavelength** Thermal and cold neutrons have wavelength comparable to interatomic spacings in solid and liquid, and elementary excitations in solids.
- **Quantitative experiments** Neutron scattering data can be used to compare to theoretical models with high precision.

Theory of Neutron Scattering

Neutrons exhibit particle-wave duality. The wave nature of a neutron allows the kinetic energy, E_n , of a neutron to be expressed in *de Broglie* wavelength, λ_n [35, 17].

$$E_n = \frac{1}{2} m_n v_n^2 = \frac{\hbar^2}{2m_n \lambda_n^2} \quad E_n [\text{meV}] = \frac{81.8042}{\lambda_n [\text{\AA}]^2} \quad (1)$$

where m_n is the mass of neutron, v_n is the velocity of the neutron, and \hbar is the Planck's constant.

Neutron scattering is described by conservation of momentum and energy between the incident and scattered neutron and the scattering object:

$$\mathbf{Q} = \mathbf{k}_i - \mathbf{k}_f \quad E = E_f - E_i = \frac{\hbar^2 k_i^2}{2m_n} - \frac{\hbar^2 k_f^2}{2m_n} \quad (2)$$

where \mathbf{Q} is the momentum transfer, \mathbf{k}_i is the initial wavevector and \mathbf{k}_f is the final wavevector, E is the energy transfer, E_i is the incident energy and E_f is the final energy [11].

Neutrons can be scattered elastically or inelastically.

- ① **Elastic scattering** happens when the scattering of neutrons happens with no change in the energy of the incident neutron [30]. It obeys Bragg's law [30], which reveals the static structure of crystalline solids, gases, liquids or amorphous materials.

$$n\lambda_n = 2d \sin \theta \quad (3)$$

where n is the diffraction order, d is the interatomic spacing and θ is the angle measured from the surface normal.

Example: neutron diffraction, neutron reflectometry, small angle neutron scattering

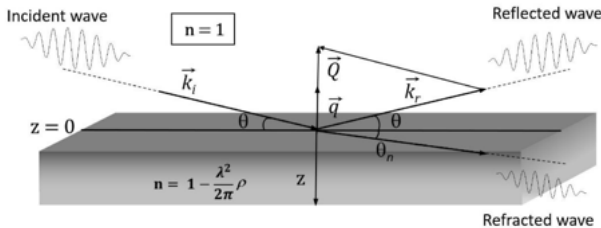
- ② **Inelastic scattering** happens when there is an exchange of energy and momentum between the incident neutron and sample, which causes both the direction and the magnitude of the wave vector to change. The energy transfer of the scattered neutrons equal to a quantum of phonon energy, $h\nu$ [35]. The energy of the neutron can be analyzed to study the vibrational motion in atoms and molecules.

Example: neutron spectroscopy, neutron spin echo, neutron backscattering

Neutron Reflectometry

Neutron reflectometry (NREF) is a powerful elastic neutron scattering technique that probes the structures of surfaces and thin films (\AA to sub- μm).

- It enables the measurements of the neutron scattering length density (SLD) profile perpendicular to the plane of a surface or an interface [5].
- The SLD profile provides information on the thickness and the chemical composition of one or several thin layers at a surface or an interface.
- Neutrons are sensitive to surfaces or interfacial structures when they impinge on the surface at sufficiently low glancing angles.



The neutron refractive index n of a medium

$$n \approx 1 - \frac{\lambda^2}{2\pi}\rho \quad (4)$$

where $\rho = Nb$ is the neutron scattering length density, N is the number density and b is the neutron scattering length [5].

The refraction of neutrons is described by the Snell-Descartes law [5, 23]:

$$\cos \theta = n \cos \theta_n \quad (5)$$

where θ is the glancing angle, θ_n is the refracted angle and n is the neutron refractive index of a medium.

The critical angle for total reflection θ_c ($\theta_n = 0$) [5, 23] after plugging Equation 4 into Equation 5, becomes [5]:

$$\cos \theta_c = n \rightarrow \sin \theta_c = \sqrt{\frac{\rho}{\pi}}\lambda \quad (6)$$

In the event when $n > 1$, total reflection cannot occur.

The reflection coefficient R is the ratio of the intensity of the reflected beam, B to the intensity of the incident beam A . The reflection coefficient can also be expressed in terms of the projection of the scattering vector on depth z , q [6, 24].

$$R = \frac{|B|^2}{|A|^2} = \left| \frac{1 - \left(1 - \left(\frac{q_c}{q}\right)^2\right)^{1/2}}{1 + \left(1 - \left(\frac{q_c}{q}\right)^2\right)^{1/2}} \right|^2 \quad R \approx \frac{16\pi^2}{q^4} \rho^2 \quad (q \gg q_c) \quad (7)$$

where q_c and q are obtained from:

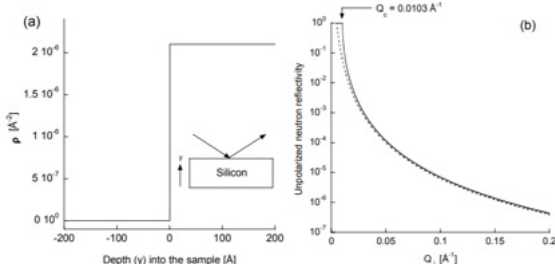
$$q = \frac{4\pi}{\lambda} \sin \theta; \quad q_c = \sqrt{16\pi\rho} \quad (8)$$

q_c is the critical scattering vector. Total reflection occurs below q_c and partial reflection occurs above q_c .

Calculating the reflectivity for a system with one or more layers requires a general technique such as the optical matrix method. This method is described by Parratt [22].

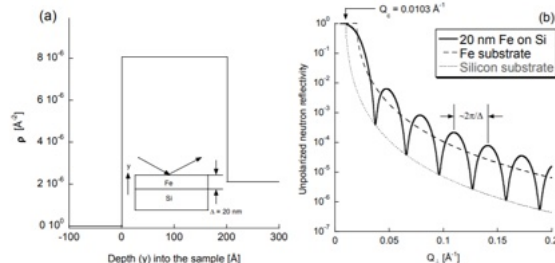
- A homogeneous silicon substrate**

When the interface between two media is smooth, there is a sharp discontinuity of SLD at the critical scattering angle q_c when passing from one layer to another.



- A thin layer of iron on a silicon substrate**

The two reflected waves from iron and silicon interfere with one another and form interference fringes (Kiessig fringes).



Motivation

- The neutron reflectometers such as SNS Liquid Reflectometer and Magnetism Reflectometer are underserved by the current detector technology, ^3He -based Multi-Wire Proportional Chamber (MWPC).
- The neutron flux is attenuated by 3 orders of magnitude to prevent count rate saturation in MWPC. Thus, the potential of the high-intensity neutron flux at SNS has not been fully maximized.
- It is expected that the neutron reflectometers in the upcoming Second Target Station (STS) will have even higher neutron flux following the Proton Power Upgrade (PPU).

Project Goal

Develop a high-rate neutron detector based on the detector requirements for neutron reflectometry instruments.

Detector Rate Challenge

- Neutron reflectometers have a high rate requirement because direct beam measurement is part of the measurements needed for a reflectivity experiment.
- Therefore, the rate requirement for neutron reflectometers is higher than some of the other scattering instruments where the measurement of the direct beam is not necessary.
- Currently, there are no detectors designed for neutron reflectometers at SNS that could handle the high neutron flux from the direct neutron beam.
- Overcoming the bottleneck of rate limitation while meeting the rest of the detector requirements is a very challenging problem.

Detector Requirements

The First Target Station (FTS) has:

- the Liquid Reflectometer (LIQREF)
- the Magnetism Reflectometer (MAGREF)

The Second Target Station (STS) is expected to have:

- the Magnetism-Second Target Advanced Reflectometer (M-STAR)
- the Quite Intense Kinetics Reflectometer (QIKR)
- the Variable Beam Profile Reflectometer (VBPR)

Requirement	LIQREF	MAGREF	M-STAR	QIKR	VBPR
Rate capability (MHz)	1	1	10	10	10
Detector efficiency at 2 Å (%)	≥ 60				
Active area (cm ²)	20×20	20×20	50×50	20×20	20×20
Gamma rejection	1×10^{-6}				
Spatial resolution (mm)	1 - 2	1 - 2	1 - 2	1 - 2	1.5
Neutron wavelength (Å)	2.5 - 17	1.8 - 14	2 - 40	2.5 - 26	2.5 - 26

Prior Similar Work

A list of potential neutron detectors for neutron reflectometry and small angle neutron scattering (SANS) instruments:

- ^3He -based Multi-Wire Proportional Chamber (MWPC)
- ^{10}B -based Multi-Blade detector (Multi-Blade) [27, 28, 29]
- Solid State Neutron Detector (SoNDe) [13, 14, 4, 31]
- Boron Array Neutron Detector (BAND-GEM) [18, 1]

Parameters	MWPC	Multi-Blade	SoNDe	BAND-GEM
Counting rate	✗	✓	✗	✓
Detection efficiency	✓	✓	✓	✗
Spatial resolution	✓	✓(x) ✗(y)	✗	✗
γ -sensitivity	✓	✓	✓	✓

Outline

① Introduction

② Detector Design and Construction

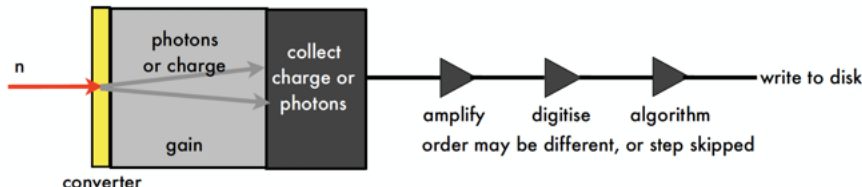
③ Detector Characterization

④ Reflectivity Experiment

⑤ Conclusion

Neutron Detectors

A neutron detector consists of:



- ① **Neutron converting layer** are materials that can convert a neutron into photons or charged particles via a neutron capture reaction.
E.g. ^3He gas, ^6Li scintillator, $^{10}\text{B}_4\text{C}$ layers, etc.
- ② **Detector/Sensor** detects photons or charged particles and transform them into current pulses.
E.g. photomultiplier tube (PMT), silicon photomultiplier (SiPM), proportional chamber, gas electron multiplier (GEM), etc.
- ③ **Readout electronics** process the electrical signals using (analog/digital) electronic circuits with associated firmware and software.

Pixelated Design: Why It Is Fast

The detector is a scintillation-based detector:

scintillator → photodetector → readout electronics

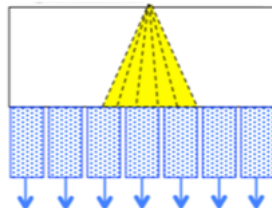
The detector adopts a pixelated design:

- The scintillator is segmented into an array of scintillator elements.
- Each scintillator element is coupled to its own photosensor.
- The output of each photosensor is read out and processed independently.

Each pixel is fully functional on its own, independent of adjacent pixels.

Comparing pixelated design to other designs:

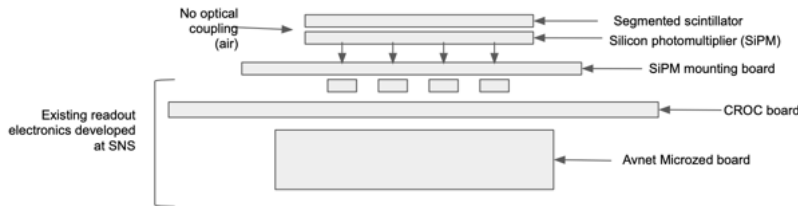
- Unsegmented scintillator
- Multiplexing readout (e.g. Anger logic, charge-division, etc)



First Detector Prototype (Proof-of-Concept)

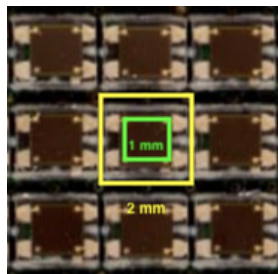
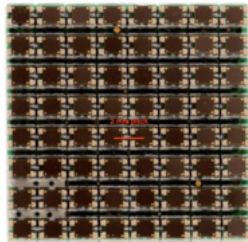
The detector consists of:

- Scintillator: 6Li glass scintillator (segmented)
 - Ce-activated lithium aluminosilicate glass (GS20, Scintacor)
 - Fast decay time between 50 to 70 ns [32]
 - Peak emission wavelength of 395 nm.
 - Thermal neutron capture: 75% (1 mm) and 95% (2 mm)
- Photodetector: Silicon photomultiplier arrays
- Readout electronics: Existing electronics at SNS



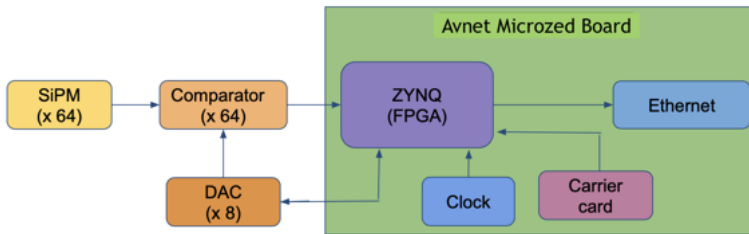
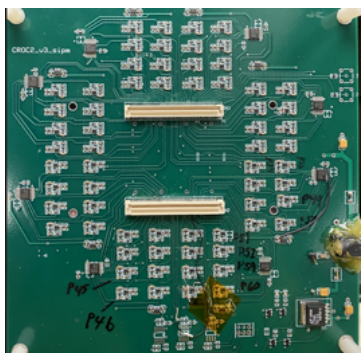
The photodetector was the ArrayC-10035064P-BGA from SensL (Cork, Ireland).

- It is an 8×8 array of SiPM sensor elements (MicroFC-10035-SMT) on a printed circuit board (PCB) with ball grid array (BGA) I/O interface [20].
- The photon detection efficiency at 395 nm is around 30% with an overvoltage of 2.5 V .
- The SiPM array itself has a pitch of 2 mm , which makes the size of a pixel to be $2.2 \times 2.2 \text{ mm}^2$
- The active area of a SiPM is $1 \times 1 \text{ mm}^2$, which is 25% of the pixel size.



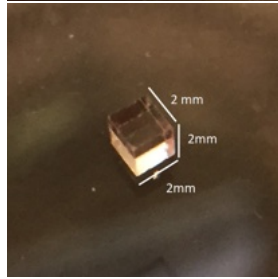
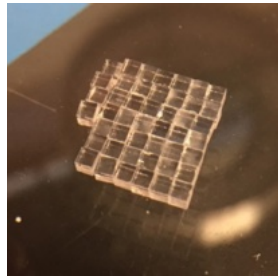
For the electronic readout, we used the Channel Read-Out-Card (CROC).

- consists of 64 comparators to perform pulse height discrimination (PHD)
- the comparator is triggered when the amplitude of a signal exceeds a certain threshold.
- Time-over-Threshold (ToT) was programmed in the firmware to improve neutron/ γ discrimination.

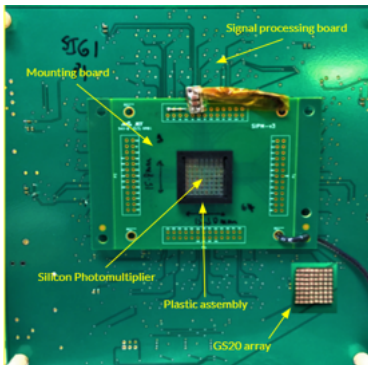


First Prototype: Construction and Assembly

- A 2" × 2" piece of GS20 scintillator was cut in-house into scintillator cubes of size 2 mm × 2 mm × 2 mm.
- Each scintillator cube was polished first by coarse grating paper (5 mm), then by fine grating paper (0.5 μm) to accomplish polished finishes.
- Reflective coating (Saint-Gobain Crystals BC-620) [12] was painted on all 5 surfaces of the scintillator cube, leaving only 1 surface that was coupled to the SiPM unpainted.
- Reflective coating was applied to maximize the light output from the scintillator and to minimize crosstalk between adjacent pixels.



- Scintillator elements were assembled in an 8×8 array and coupled to the SiPM without optical grease/layer.
- Each individual channel in the SiPM was read out independently using a custom-made mounting board that acts as an interface between the SiPM array and the readout system (the CROC board).
- The SiPM signals were fed into the CROC board for signal processing. The data were then sent to a computer via an Ethernet connection.
- The SiPM was biased at 27.5 V with a discrimination threshold of 500 (arb. unit) for all channels. The CROC board and the Avnet Microzed board were powered up with 5 V.



Modifications for Second Detector Prototype

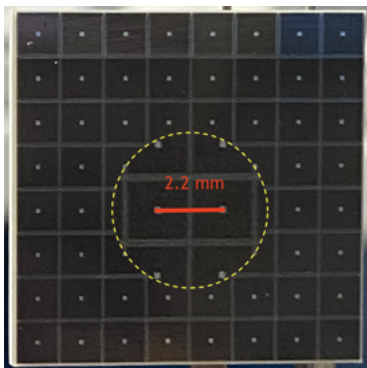
There are four main areas of improvements for the second prototype:

- ① Ability to Scale Up** The final detector should have an active area of $20 \times 20 \text{ cm}^2$. Currently, the active area of the first detector prototype is $16 \times 16 \text{ mm}^2$, but it is not easily scalable.
- ② Discontinuation of the SiPM model** The SiPM was discontinued in production after company acquisition. An alternative SiPM model that is commercially readily available and quality assured is needed to replace the current model.
- ③ Mass Production of GS20 Scintillator Arrays** The fabrication of the scintillator arrays was a long and tedious process. Collaboration with external companies was desired to obtain consistently high-quality scintillator arrays in large quantities
- ④ Ability to Perform Neutron Reflectivity Experiment** The detector area was expanded to obtain sufficient detector area coverage for a neutron reflectivity experiment.

Second Detector Prototype

The neutron scintillator remains GS20 from Scintacor. The SiPM has been replaced with the Hamamatsu S13361-2050AE-08 Multi-Pixel Photon Counter (MPPC) array.

- It is an 8×8 array on a printed circuit board with a connector made by SAMTEC mounted on the back side of the board [25].
- The photon detection efficiency at 395 nm is about 40% with an overvoltage of 3.0 V .
- The MPPC array has a pitch of 2.2 mm , which makes the size of a pixel to be $2.2 \times 2.2 \text{ mm}^2$.
- The effective photosensitive area for each channel is $2 \times 2 \text{ mm}^2$, which is about 82% of the size of a pixel [25].



Comparison between SensL ArrayC-10035064P-BGA SiPM (shortened as SensL SiPM) and Hamamatsu S13361-2050AE-08 MPPC array (shortened as Hamamatsu MPPC).

Similarities:

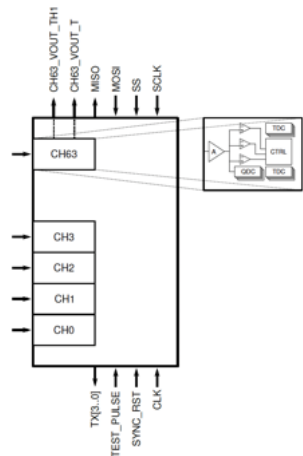
	SensL SiPM	Hamamatsu MPPC
Number of pixels	8×8	8×8
Array pitch (mm)	2.0	2.2
Spectral range, λ (nm)	300 - 950	320 - 900
Peak wavelength, λ_p (nm)	420	450

Differences:

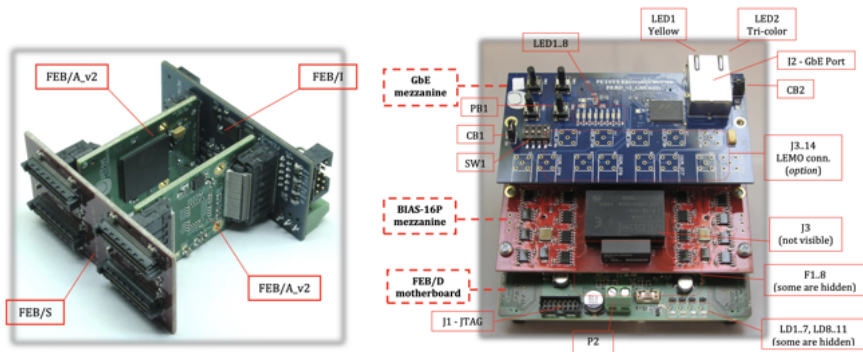
	SensL SiPM	Hamamatsu MPPC
Photosensitive area/channel (mm^2)	1×1	2×2
Dead space between pixels (mm)	1.0	0.2
Breakdown voltage, V_{br} (V)	24.2 - 24.7	53 ± 5
Dark count rate, DCR (kHz)	30	300
Photon detection efficiency, PDE (%)	31	40

The CROC board was replaced with the PETsys readout system, which is designed to read a large number of SiPM channels with a high data rate and excellent time resolution [10].

- Based on the TOFPET2 ASIC [9]: Signal amplification and discrimination for each of 64 independent channels. [9].
- Offers two modes of measurement: time and charge (QCD) mode and dual time (ToT) mode [9].
- Has a dynamic range of 1500 pC , which is suitable for SiPMs
- Separately configurable thresholds for each channel is possible
- Maximum event rate*: 15 Mcps (Gbit Ethernet) and 100 Mcps (SFP+)
- Compatible with external synchronization [10].

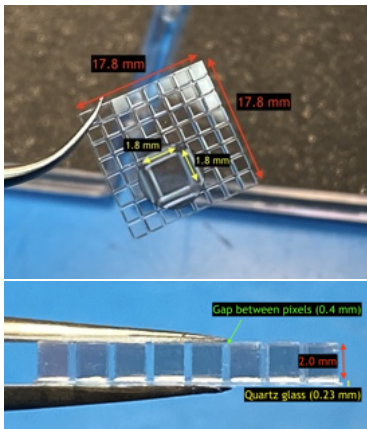


The evaluation kit includes two Front-End Modules (FEM128), one Front-End type D module (FEB/D-1024), firmware for the FEB/D board and application software for data acquisition [8].

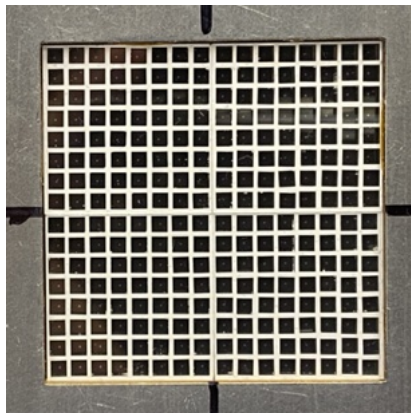


Second Prototype: Construction and Assembly

- Each element in the scintillator array is $1.8 \times 1.8 \times 2.0 \text{ mm}^3$ in size. All surfaces have polished finishes.
- The scintillator elements were aligned at a pitch of 2.2 mm , following the pitch of the SiPM array.
- These scintillator elements were then glued to a thin piece of 0.23 mm thick quartz glass to form a $17.8 \times 17.8 \times 2.23 \text{ mm}^3$ scintillator array.
- The scintillator arrays were fabricated by our collaborator (IRD Glass)



To prevent crosstalk across adjacent pixels, a reflective coating (Avian-B) was applied to all surfaces but the top and bottom surfaces. An aluminum fixture was custom-made to hold the scintillator arrays in place. No optical coupling was applied. The gap between adjacent pixels is 0.4 mm.

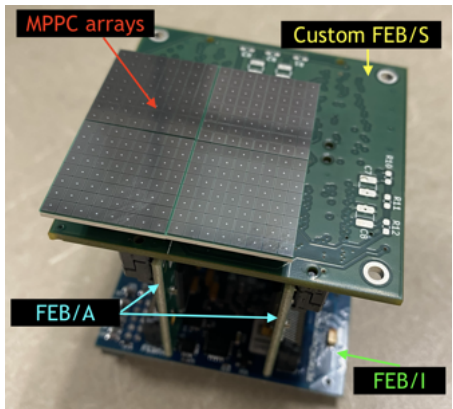


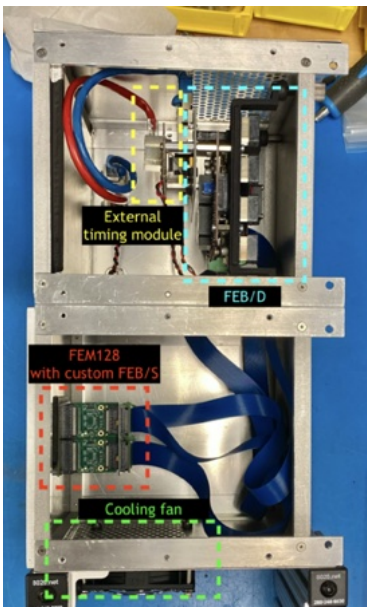
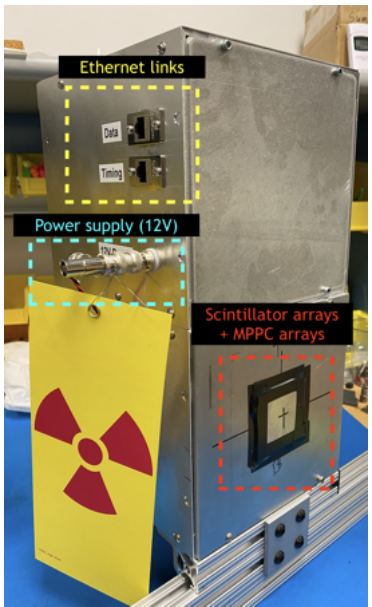
To integrate MPPC arrays to the PETsys readout system,

- The FEB/S board had to be redesigned because the SiPM arrays used are different models and cannot be directly mounted to the original FEB/S board.
- The custom FEB/S was then connected to FEM128 modules and the rest of the PETsys SiPM readout system.

Operational settings:

- The whole detector was powered up with a 12 V supply.
- The MPPC arrays were biased at 53 V with an overvoltage of 4 V.
- The time and charge (QCD) mode was used for acquisition. The thresholds for time (v_{t1}) and charge (v_e) were set at 20 and 27, respectively.





There are four main areas of modifications in the second prototype:

- ① Ability to Scale Up:** The CROC board was replaced with PETsys readout system. The use of ASIC chips reduces the size of the electronics significantly. The replacement allows the detector system to scale without significant modifications to the system.
- ② Replacement of the SiPM model:** The SensL SiPM was substituted with the Hamamatsu MPPC arrays. With the changes, the active area per pixel is larger with smaller dead space.
- ③ Production of GS20 Scintillator Arrays:** The scintillator arrays were fabricated in collaboration with IRD Glass, which produced consistently high-quality scintillator arrays with high precision in alignment.
- ④ Ability to Perform Neutron Reflectivity Experiment:** The detector area was expanded from $16 \times 16 \text{ mm}^2$ to $35.6 \times 35.6 \text{ mm}^2$, which is a sufficient detector area coverage. An external timing module was added to synchronize the PETsys system clock with the accelerator pulse for time-of-flight (ToF) measurements in reflectivity experiments.

Outline

- ① Introduction
- ② Detector Design and Construction
- ③ Detector Characterization
- ④ Reflectivity Experiment
- ⑤ Conclusion

Detector Characterization

A series of tests was performed on both prototypes. These tests include neutron detection efficiency, counting rate, γ -sensitivity, spatial resolution and crosstalk.

A calibrated ^{60}Co γ source was used for the γ -sensitivity test.

The ^{60}Co main photon energies are 1.173 MeV (99.85%) and 1.332 MeV (99.98%).

Neutron source	Neutron wavelength (\AA)	Wave-length (\AA)
High-Resolution Neutron Powder Diffractometer (PSD), MURR	1.48	
Double-Axis Powder Diffractometer (2X-C), MURR	4.33	
Instrument Development Beamline (CG-1A), HFIR	4.22	
Detector lab, SNS	moderated ^{252}Cf	

Neutron Detection Efficiency

In order to calibrate the neutron flux, a $1 - \text{inch}$ diameter ${}^3\text{He}$ gas detector filled with 8 bars of ${}^3\text{He}$ and 1 bar CF_4 was used to measure the neutron flux. The ${}^3\text{He}$ detector was assumed to have a detection efficiency close to 100% at the neutron wavelengths of the beam lines.

The relative detection efficiency, ϵ can be calculated by taking the ratio of the number of counts measured by the pixelated detector, $N_{\text{pixelated}}$ over the number of counts measured by the ${}^3\text{He}$ detector, $N_{{}^3\text{He}}$.

$$\epsilon = \frac{N_{\text{pixelated}}}{N_{{}^3\text{He}}} \quad (9)$$

A mask aperture of $1 \times 1 \text{ cm}^2$ was used to make sure the detector active area remains the same for both detectors. These two quantities need to be normalized by acquisition time and background-subtracted prior to taking the ratio.

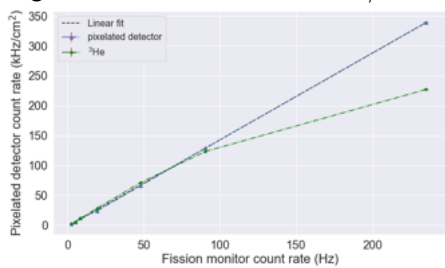
First prototype: 75% (1.8 \AA) and 92% (4.2 \AA)

Second prototype: 62% (4.2 \AA)

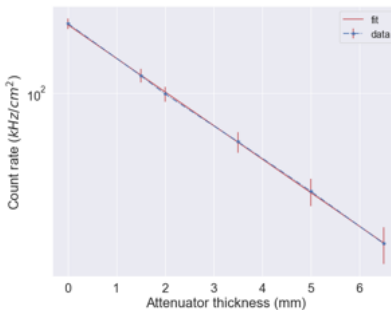
Counting Rate

To measure the maximum counting rate capability of the detector, multiple attenuators of varying thicknesses were used to attenuate the neutron flux to different intensities. A fission monitor, that has a very low detection efficiency, was used as a reference during the test to observe any count rate saturation on the detector of interest.

First detector prototype
Highest measured rate: 392 kHz/cm^2



Second detector prototype
Highest measured rate: 225 kHz/cm^2



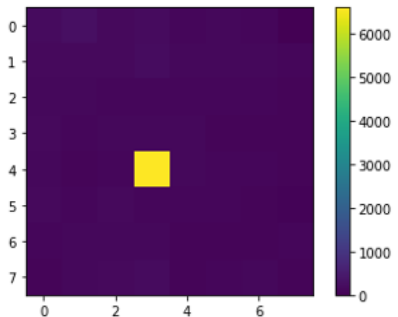
Crosstalk

To measure the detector overall crosstalk, a piece of borated aluminum with a $1 - \text{mm}$ diameter hole was centered over a pixel. The crosstalk was approximated using the following formula:

$$\text{crosstalk (\%)} = \frac{\bar{N}_{\text{first nearest neighbors}} - \bar{N}_{\text{second nearest neighbors}}}{N_{\text{target pixel}}} \times 100 \quad (10)$$

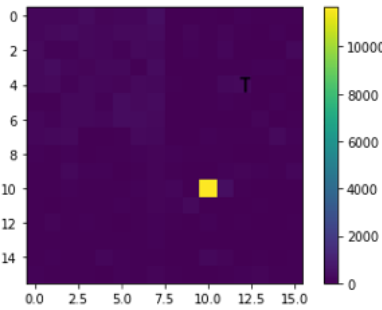
First detector prototype

Crosstalk: $\leq 3\%$



Second detector prototype

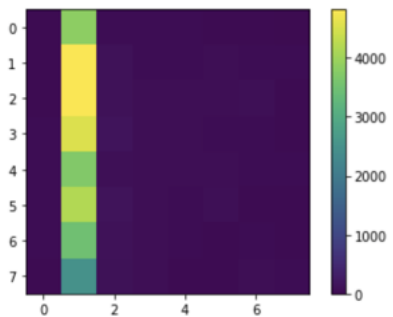
Crosstalk: $\leq 1\%$



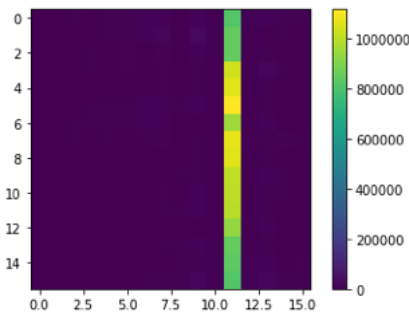
Spatial Resolution

The spatial resolution of the detector is largely determined by the pitch of the sensor array. To measure the spatial resolution of the detector, a borated aluminum mask with a slit was used.

First detector prototype
spatial resolution: 2 mm
slit width: 0.85 mm



Second detector prototype
spatial resolution: 2.2 mm
slit width: 1.5 mm



γ sensitivity

The gamma sensitivity is defined as the ratio of the number of counts measured using the detector, N_{detected} to the number of γ -rays incident at the detector, N_{incident} . N_{incident} can be derived from the number of γ -rays emitted from the γ source, N_{emitted} multiplied by the solid angle ω subtended by the detector from the γ source.

$$\gamma - \text{sensitivity} = \frac{N_{\text{detected}}}{N_{\text{incident}}} \quad (11)$$

The solid angle, ω subtended by a rectangular area of size $l \times b$ at any point lying on the perpendicular axis at a distance, d away from the center of the source is given by:

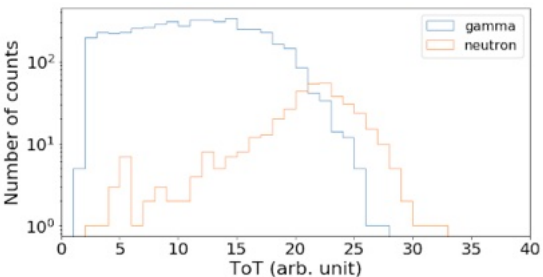
$$\omega = 4\sin^{-1} \left(\frac{lb}{\sqrt{(l^2 + 4d^2)(b^2 + 4d^2)}} \right) \quad (12)$$

First prototype: 1×10^{-3} (pulse height discrimination, PHD) and 1×10^{-4} (Time-over-Threshold, ToT)

Second prototype: 1×10^{-2} (charge integration, QCD)

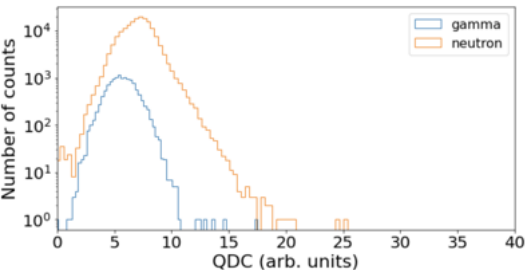
First prototype:

- Pulse height discrimination
- Time-over-Threshold (ToT)



Second prototype:

- Charge integration (QCD)



Summary

Comparison in detector performance between the first prototype and the second prototype.

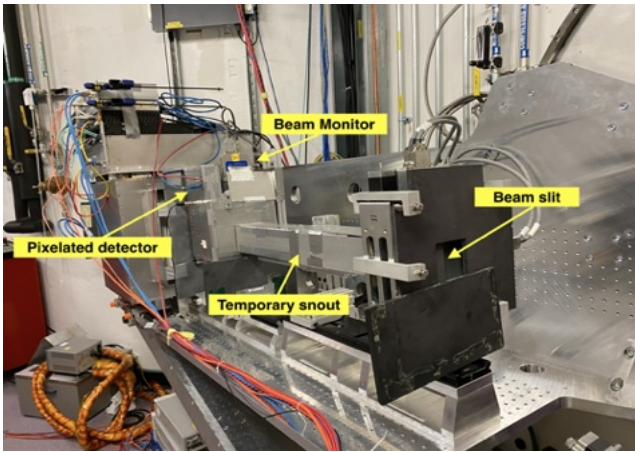
Parameters	First prototype	Second prototype
Counting rate (kHz/cm ²)	≥ 392	≥ 225
Neutron efficiency relative to ³ He detector (%)	92 (4.2 Å) 75 (1.8 Å)	62 (4.2 Å)
Spatial resolution (mm)	2.0	2.2
Crosstalk (%)	≤ 3	≤ 1
Active area (cm ²)	1.6 × 1.6	3.56 × 3.56
Gamma sensitivity	1 × 10 ⁻³ (PHD) 1 × 10 ⁻⁴ (ToT)	1 × 10 ⁻² (QDC)

Outline

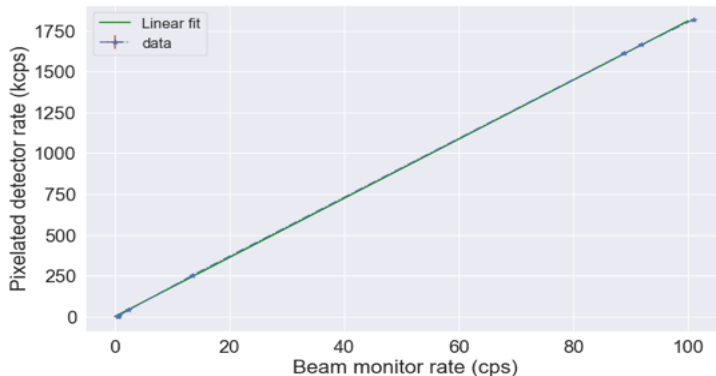
- ① Introduction**
- ② Detector Design and Construction**
- ③ Detector Characterization**
- ④ Reflectivity Experiment**
- ⑤ Conclusion**

Counting Rate Test

Since a reactor has a different neutron profile than a spallation source, it is important to characterize the instantaneous count rate capability of the detector.



- The instrument was adjusted such that the angle of the sample was set to 0° .
- To vary the neutron flux at the instrument, the number of attenuators (borated polyethylene) was varied at the beam port
- A beam monitor (Ordela Model 4515-N-L) [21] was used as a benchmark for linearity

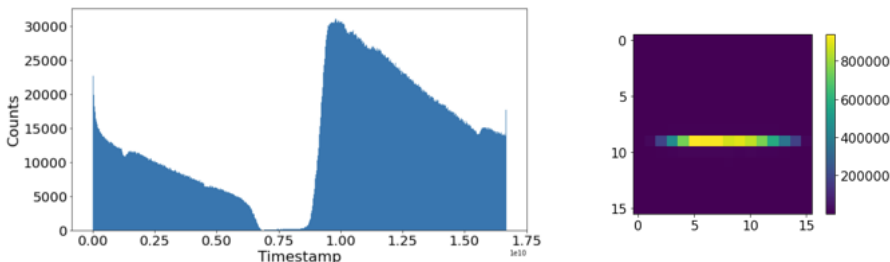


The instantaneous count rate is defined as the number of counts recorded per the time bin in a single frame over the whole detector area. The local instantaneous rate is defined by the instantaneous count rate per pixel.

$$\text{instantaneous rate} = \frac{\text{Number of counts}}{\text{bin size} \times \text{number of frames}} \quad (13)$$

The highest instantaneous rate of the detector was about 1.03 Mcps.

The highest local instantaneous rate was about 83.5 kcps/pixel (17.3 kcps/mm² or 1.73 Mcps/cm²).



Each frame is approximately 16.67 ms. In a single time frame, there are 814 time bins with a bin size of 20.48 μ s.

Conclusion for Counting Rate Test

- The outcome of the counting rate test was **significant**.
- The pixelated detector demonstrated a high counting rate capability with no dead time at the highest neutron flux setting (without any attenuators).
- The ability to make direct beam measurements without attenuators has *never* been achieved by the current detector, MWPC.
- This can not only drastically reduce the time needed for an experiment, but also overcome the bottleneck of rate-limited neutron reflectivity experiments.

Neutron Reflectivity Experiment at BL-4B

For the neutron reflectivity experiments, it is important to evaluate the performance of the detector in actual experimental conditions. The same experiments were repeated using MWPC as a benchmark.

Two standard samples, namely iridium on silicon wafer and quartz, were used.

- **Quartz** has a well-known critical angle
- **Iridium on silicon** produces a reflectivity curve with well-defined interference fringes

At BL-4B, a neutron reflectivity experiment consists of:

- A set of measurements for direct beam and reflected beam.
- Seven different instrument configurations were needed to get a full reflectivity curve over a range of scattering vectors ($0.008 < Q < 0.3 \text{ \AA}^{-1}$).
- The neutron wavelength was varied for the first 5 runs, and the sample angle was changed for the last 2 runs.

Direct Beam Configuration

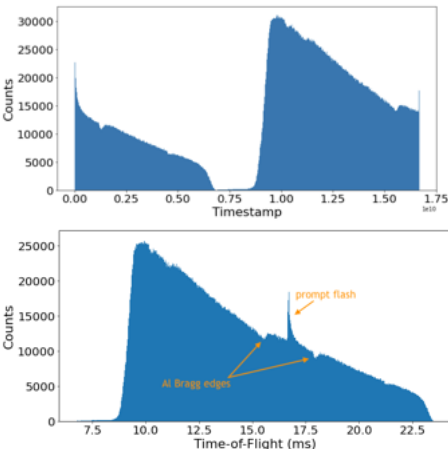
run	central neutron wavelength (Å)	sample angle (°)	detector angle (°)	acquisition time (s)
1	15.000	0.0	0.0	900
2	12.386	0.0	0.0	900
3	9.740	0.0	0.0	900
4	7.043	0.0	0.0	300
5	4.250	0.0	0.0	300
6	4.250	0.0	0.0	300
7	4.250	0.0	0.0	300

Reflected Beam Configuration

run	central neutron wavelength (Å)	sample angle (°)	detector angle (°)	acquisition time (s)
1	15.000	0.600	1.200	300
2	12.386	0.600	1.200	300
3	9.740	0.600	1.200	300
4	7.043	0.600	1.200	300
5	4.250	0.600	1.200	300
6	4.250	1.183	2.366	600
7	4.250	2.343	4.686	4030

Data Acquisition

- The timestamp, energy and pixel ID for each event were stored. The timestamps for the rising and falling edge of the accelerator pulse were also recorded.
- The Bragg edges from aluminum were observed in the ToF spectrum as expected since there were aluminum materials used at the beam line.
- Because of the difference in neutron energies, some neutrons made it to the detector within the same frame, but others were captured in the subsequent frame. The distance between the moderator and the detector is 15.09 m.
- At 0.0 s (in unshifted ToF spectrum) or 16.67 ms (in shifted ToF spectrum), the proton beam hit the target.



Reflectivity Analysis

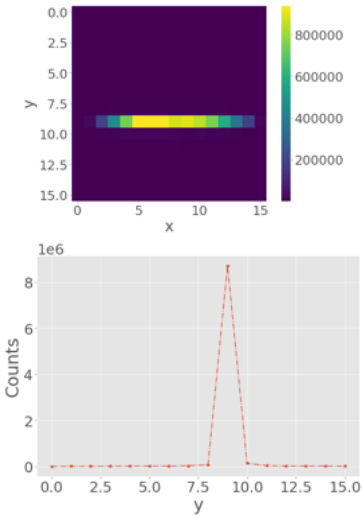
This analysis focuses on specular reflectivity:

- Only background-subtracted events from the narrow region (row 9) were used.
- Events that fell within the prompt pulse region were disregarded.
- To transform ToF to scattering vector, Q :

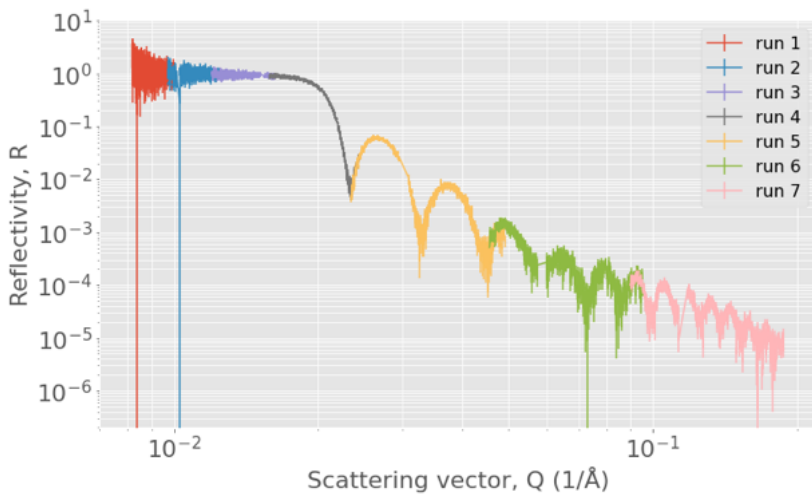
$$Q = \frac{4\pi \sin(\theta)}{\lambda} \quad \lambda [\text{\AA}] = \frac{3956}{v [\text{m/s}]} \quad v = \frac{d}{\text{ToF}} \quad (14)$$

- Data were normalized with the proton charge of the accelerator pulse because the amount of charge hitting the target affects the number of neutrons produced.
- Reflectivity $R(Q)$ was obtained:

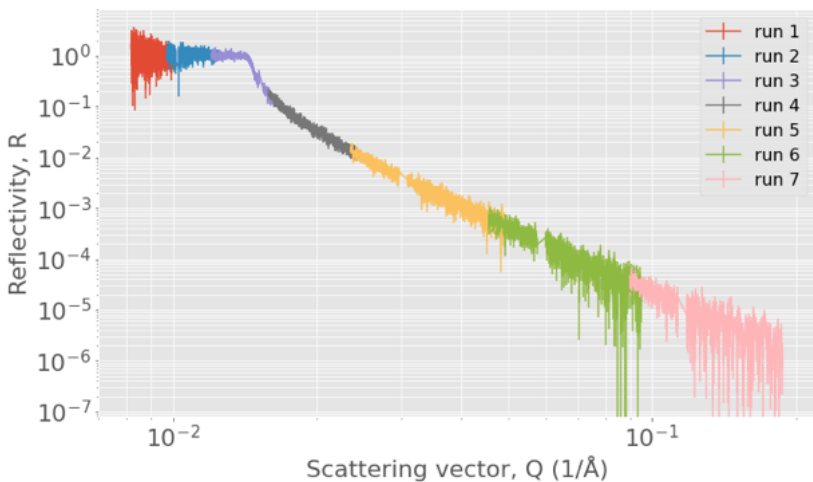
$$R(Q) = \frac{N_{\text{reflected}}(Q)}{N_{\text{direct}}(Q)} \quad (15)$$



Reflectivity curve for iridium sample



Reflectivity curve for quartz sample



Reflectivity Fitting

To transform the reflectivity curve to scattering length density (SLD) profile, the reflectivity measurements were modeled using a reflectivity fitting software [15, 7].

- Define an initial SLD profile. The SLD profile is made up of a series of layers.
- Each layer is defined by thickness, a uniform SLD and roughness.
- Once the initial SLD was properly set up, the reflectivity was computed for the SLD profile and compared with the measured reflectivity.
- It is important to have prior knowledge about the sample composition to obtain an accurate and reliable SLD.

Layer Models

Iridium

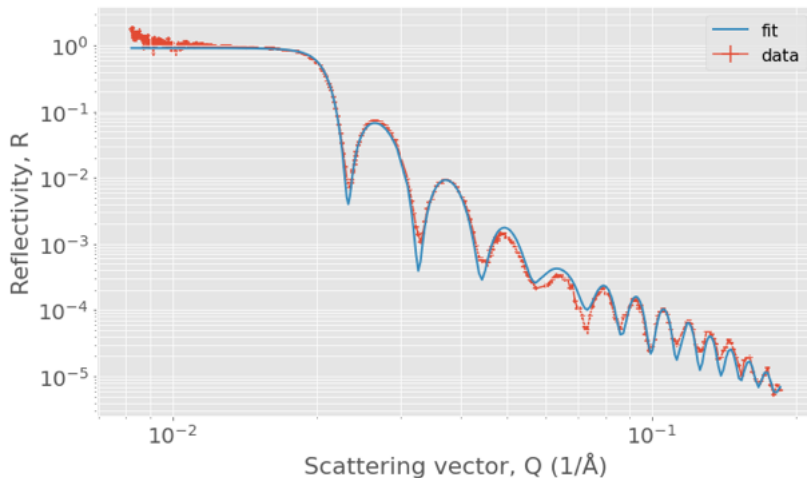
Layer	Thickness (Å)	SLD ($10^{-6}/\text{\AA}^2$)	Roughness (Å)
Air	-	0.0	-
Iridium oxide	48.68	3.807	22.76
Iridium	457.2	7.153	6.786
Silicon oxide	18.12	0.048	1.309
Silicon	-	2.07	0.691

Quartz

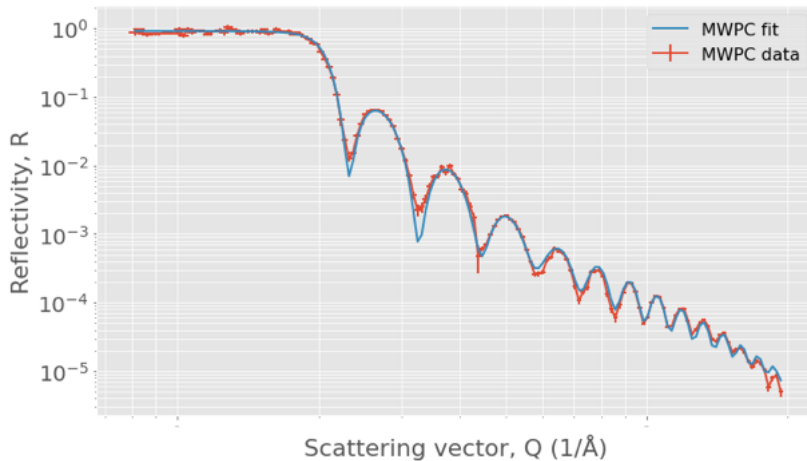
Layer	Thickness (Å)	SLD ($10^{-6}/\text{\AA}^2$)	Roughness (Å)
Air	-	0.0	-
Quartz	-	4.068	1.012

The reflectivity fitting program was run using the Nelder-Mead algorithm as its fitting engine [19]. The objective of the fitting engine was to minimize the least-square difference between the computed reflectivity and the measured reflectivity.

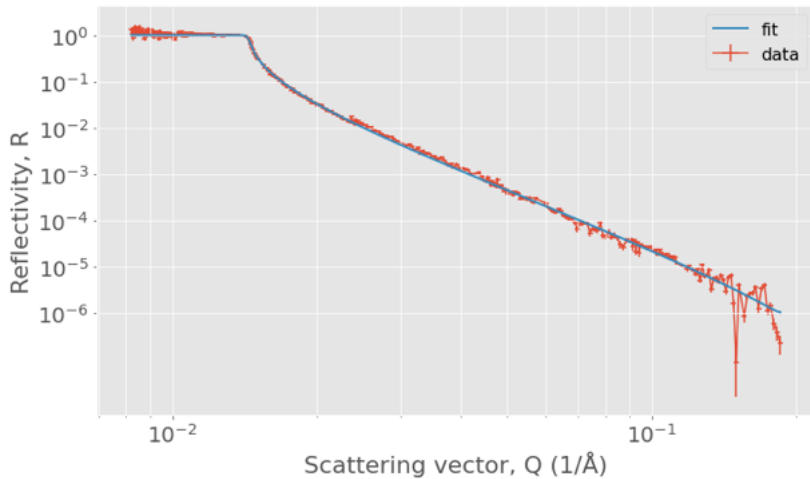
Computed and Measured Reflectivity Curve for Iridium Using Pixelated Neutron Detector (PiNDe)



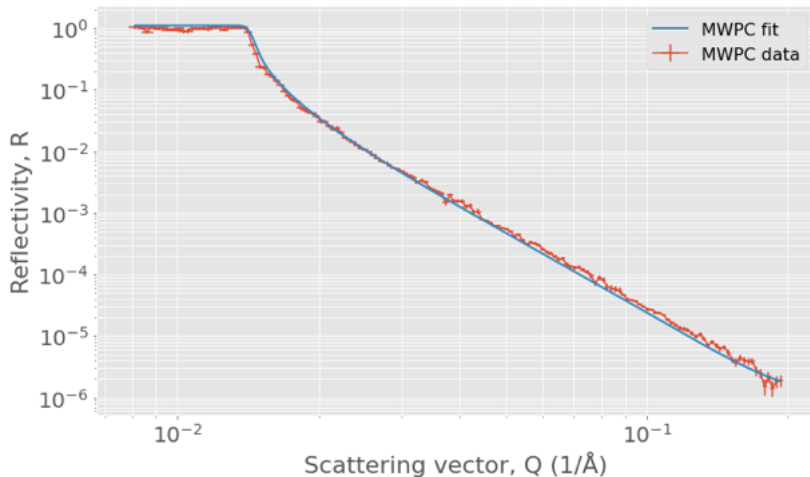
Computed and Measured Reflectivity Curve for Iridium Using MWPC



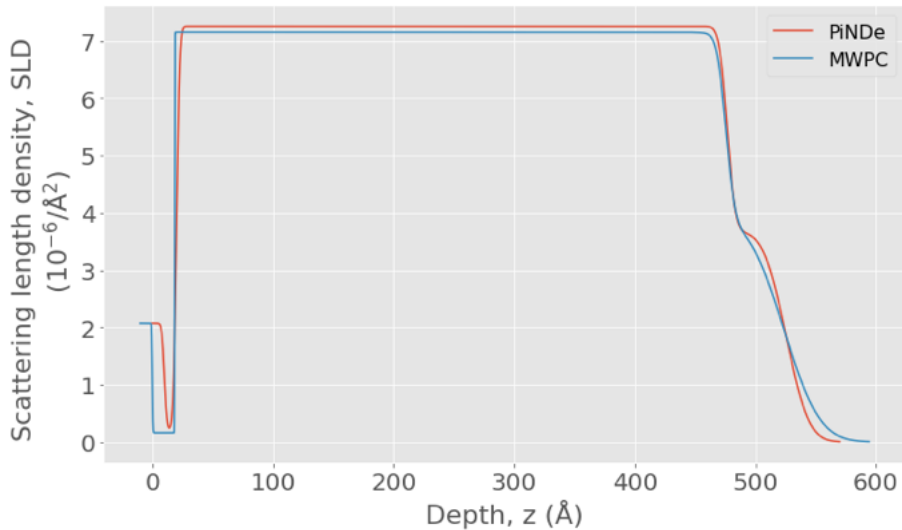
Computed and Measured Reflectivity Curve for Quartz Using PiNDe



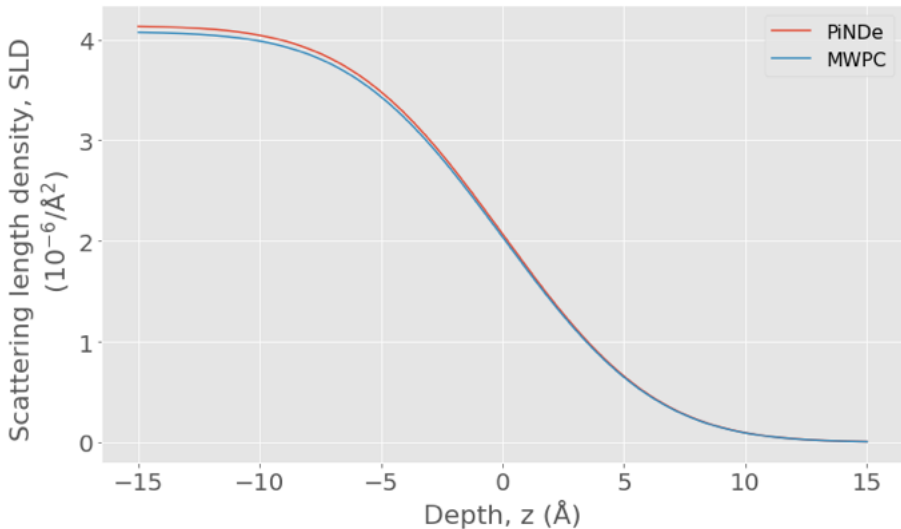
Computed and Measured Reflectivity Curve for Quartz Using MWPC



Scattering Length Density (SLD) Profile for Iridium



Scattering Length Density (SLD) Profile for Quartz



Quantitative Evaluation of SLD

Parameter	Iridium		Percent difference (%)
	MWPC	PiNDe	
iridium oxide layer			
thickness (Å)	48.11	48.51	0.825
SLD ($10^{-6}/\text{\AA}^2$)	3.933	3.663	7.371
roughness (Å)	23.53	14.13	66.525
iridium layer			
thickness (Å)	456.9	456.2	0.153
SLD ($10^{-6}/\text{\AA}^2$)	7.151	7.256	1.447
roughness (Å)	5.991	1.384	332.8
silicon oxide layer			
thickness (Å)	18.6	10.18	82.711
SLD ($10^{-6}/\text{\AA}^2$)	0.16	0.5895	72.858
roughness (Å)	0.161	2.158	92.539
goodness of fit			
χ^2	4.017	12.852	-

In terms of the quartz and iridium layers, both detectors show a close agreement with a percent difference of typically $< 1\%$ and $< 2\%$ for thickness and SLD, respectively.

Quantitative Evaluation of SLD

Parameter	Quartz		Percent difference (%)
	MWPC	PiNDe	
quartz layer			
thickness (Å)	-	-	-
SLD ($10^{-6}/\text{\AA}^2$)	4.078	4.138	1.471
roughness (Å)	-	-	-
goodness of fit			
χ^2	5.33	7.317	-

Outline

- ① Introduction
- ② Detector Design and Construction
- ③ Detector Characterization
- ④ Reflectivity Experiment
- ⑤ Conclusion

Summary Findings

- The high-rate pixelated neutron detector demonstrated its high counting rate capability from all the rate tests. The detector is capable of handling the direct beam with no dead time.

This has never been achieved before by the current detectors.

The limit of counting rate capability of the pixelated detector has not yet been determined.

- The pixelated detector produced reflectivity measurements that were in very good agreement with the reflectivity measurements obtained using MWPC.

Despite having a higher γ -sensitivity, the pixelated detector was able to capture the reflectivity oscillations in high Q region.

Comparison between the detector performance and instrument requirements

Parameters	First prototype	Second prototype	Instrument Requirement (FTS)
Global time-average count rate (cps)	$\geq 1 \times 10^6$	$\geq 1.8 \times 10^6$	1×10^6
Local time-average count rate (cps/cm^2)	$\geq 3.92 \times 10^5$	$\geq 2.25 \times 10^5$	-
Global instantaneous count rate (cps)	-	$\geq 1.03 \times 10^6$	-
Local instantaneous count rate (cps/cm^2)	-	$\geq 1.73 \times 10^6$ (83.5 kcps/pixel)	-
Neutron efficiency relative to 3He detector (%)	92 (4.2 Å) 75 (1.8 Å)	62 (4.2 Å)	≥ 60 (2.0 Å)
Spatial resolution (mm)	2.0	2.2	1-2
Crosstalk (%)	≤ 3	≤ 1	
Active area (cm^2)	1.6×1.6	3.56×3.56	20×20
Gamma sensitivity	1×10^{-3} (PHD) 1×10^{-3} (ToT)	1×10^{-2} (QDC)	1×10^{-6}

Recommended Future Work

- A rate test needs to be conducted at a beam line with more intense neutron flux to determine the maximum counting rate capability of the pixelated detector
- Although the pixelated detector performed relatively well in the reflectivity measurement, the γ sensitivity of the detector needs to be further improved.
- Since the detector area needs to be extended to a much larger area, it is important to ensure that the performance of the detector remains consistent on a larger scale.
- It would be interesting to explore a monolithic scintillator with individual readout to improve spatial resolution without compromising the rate capability too significantly.

Outline

⑥ Acknowledge

⑦ References

⑧ Appendix

Acknowledge

- I would like to thank my dissertation committee, Dr. Jason Hayward, Dr. Richard Riedel, Dr. Lawrence Heilbronn and Dr. Nicole McFarlane for the support and guidance over the years.
- I am immensely grateful to my research advisor, Dr. Richard Riedel, and members of the Detector Group at SNS such as Bruce Hannan, Cornelius Donahue, Theodore Visscher, Christopher Montcalm, Justin Beal, and Loren Funk.
- I also owe thanks to the members of the SNS Liquid Reflectometer team such as Dr. Mathieu Doucet, Candice Halbert, Dr. Jim Browning and Dr. John Ankner for all the discussion, planning and analysis related to neutron reflectivity experiments.
- Last but not least, I would not be where I am right now without the love and support from my family, close friends and my partner.
- This work is supported by the U.S. Department of Energy, Office of Sciences, Office of Basic Energy Sciences under Contract Numbers DE-AC05-00OR22725 and DE- SC0022292.

Thank you for listening!

Outline

⑥ Acknowledge

⑦ References

⑧ Appendix

References I

- [1] Giorgia Albani, Enrico Perelli Cippo, Gabriele Croci, Andrea Muraro, Richard Hall-Wilton, Carina Höglund, Alain Menelle, Giovanni Grosso, Fabrizio Murtas, Marica Rebai, et al.
High-rate measurements of the novel band-gem technology for thermal neutron detection at spallation sources.
Nuclear Instruments and Methods in Physics Research Section A: Accelerators, Spectrometers, Detectors and Associated Equipment, 957:163389, 2020.
- [2] G Blasse.
Scintillator materials.
Chemistry of Materials, 6(9):1465–1475, 1994.
- [3] Peter Böni and Albert Furrer.
Introduction to neutron scattering.
In *Neutron Scattering in Layered Copper-Oxide Superconductors*, pages 1–22. Springer, 1998.
- [4] Laura Boyd.
Characterisation of a position sensitive thermal neutron detector.
PhD thesis, University of Glasgow, 2021.
- [5] Fabrice Cousin and Giulia Fadda.
An introduction to neutron reflectometry.
In *EPJ Web of Conferences*, volume 236, page 04001. EDP Sciences, 2020.
- [6] Robert Cubitt and Giovanna Fragneto.
Neutron reflection:: Principles and examples of applications.
In *Scattering*, pages 1198–1208. Elsevier, 2002.
- [7] M. Doucet, R.M. Ferraz Leal, and T.C. Hobson.
Web interface for reflectivity fitting.
SoftwareX, 7:287–293, 2018.
- [8] PETsys Electronics.
Petsys time-of-flight asic evaluation kit.

References II

- [9] PETsys Electronics.
Petsys tofpet2 asic.
- [10] PETsys Electronics.
Sipm readout system.
- [11] Felix Fernandez-Alonso and David L Price.
Neutron Scattering: fundamentals, volume 44.
Academic Press, 2013.
- [12] Saint Gobain.
Reflector paint for plastic scintillators (bc-620) saint gobain.
- [13] Sebastian Jaksch, Ralf Engels, Günter Kemmerling, Codin Gheorghe, Philip Pahlsson, Sylvain Désert, and Frederic Ott.
Cumulative reports of the sonde project july 2017.
arXiv preprint arXiv:1707.08679, 2017.
- [14] Sebastian Jaksch, Ralf Engels, Günter Kemmerling, Uwe Clemens, Sylvain Désert, Hanno Perrey, Codin Gheorghe, Arne Fredriksen, Petter Øya, Henrich Frielinghaus, and et al.
Recent developments sonde high-flux detector project.
Proceedings of the International Conference on Neutron Optics (NOP2017), 2018.
- [15] P.A. Kienzle, K.V O'Donovan, J.F. Ankner, N.F. Berk, and C.F. Majkrzak.
Reflectometry software: Refl1d, 2015.
- [16] S. Kumar, M. Herzkamp, D. Durini, H. Nöldgen, and S. Van Waasen.
Development of a solid-state position sensitive neutron detector prototype based on 6li-glass scintillator and digital sipm arrays.
Nuclear Instruments and Methods in Physics Research Section A: Accelerators, Spectrometers, Detectors and Associated Equipment, page 161697, 2018.
- [17] Kim Lefmann.
Neutron scattering: Theory, instrumentation, and simulation.
Niels Bohr Institute, University of Copenhagen, 2017.

References III

- [18] Andrea Muraro, Gabriele Croci, Enrico Perelli Cippo, Giovanni Grosso, Carina Höglund, Giorgia Albani, Richard Hall-Wilton, Kalliopi Kanaki, Fabrizio Murtas, Davide Raspino, and et al.
Performance of the high-efficiency thermal neutron band-gem detector.
Progress of Theoretical and Experimental Physics, 2018(2), Feb 2018.
- [19] J. A. Nelder and R. Mead.
A Simplex Method for Function Minimization.
The Computer Journal, 7(4):308–313, 01 1965.
- [20] OnSemiconductor.
C-series low noise, blue-sensitive silicon photomultipliers datasheet, 2021.
- [21] Ordela.
Neutron beam monitors, Feb 2019.
- [22] Lyman G Parratt.
Surface studies of solids by total reflection of x-rays.
Physical review, 95(2):359, 1954.
- [23] J Penfold and RK Thomas.
The application of the specular reflection of neutrons to the study of surfaces and interfaces.
Journal of Physics: Condensed Matter, 2(6):1369, 1990.
- [24] Jeffrey Penfold and Robert K Thomas.
Neutron reflectivity and small angle neutron scattering: An introduction and perspective on recent progress.
Current opinion in colloid & interface science, 19(3):198–206, 2014.
- [25] Hamamatsu Photonics.
Hamamatsu mppc (multi-pixel photon counter) arrays: S13361-2050 series.
- [26] Slawomir Piatek.
Silicon photomultipliers: Operation, performance, and possible applications, 2008.

References IV

- [27] F Piscitelli, JC Buffet, JF Clergeau, S Cuccaro, B Guérard, Anton Khaplanov, Q La Manna, JM Rigal, and P Van Esch. Study of a high spatial resolution 10b-based thermal neutron detector for application in neutron reflectometry: the multi-blade prototype. *Journal of Instrumentation*, 9(03):P03007, 2014.
- [28] Francesco Piscitelli. Novel boron-10-based detectors for neutron scattering science. *The European Physical Journal Plus*, 130(2):1–9, 2015.
- [29] Francesco Piscitelli, Francesco Messi, Michail Anastopoulos, Tomasz Bryś, Faye Chicken, Eszter Dian, Janos Fuzi, Carina Höglund, Gabor Kiss, Janos Orban, et al. The multi-blade boron-10-based neutron detector for high intensity neutron reflectometry at ess. *Journal of Instrumentation*, 12(03):P03013, 2017.
- [30] Roger Pynn. Neutron scattering: A primer, 1990.
- [31] E Rofors, N Mauritson, H Perrey, R Al Jebali, JRM Annand, L Boyd, MJ Christensen, U Clemens, S Desert, R Engels, et al. Response of a li-glass/multi-anode photomultiplier detector to collimated thermal-neutron beams. *Nuclear Instruments and Methods in Physics Research Section A: Accelerators, Spectrometers, Detectors and Associated Equipment*, 999:165170, 2021.
- [32] Scintacor. An introduction to lithium-6 glass.
- [33] Scintacor. Scintacor lithium glass scintillators, 2021.
- [34] A.R Spowart. Neutron scintillating glasses: Part ii. *Nuclear Instruments and Methods*, 140:19–28, 01 1977.

References V

- [35] Igor A Zaliznyak and John M Tranquada.
Neutron scattering and its application to strongly correlated systems.
In *Strongly Correlated Systems*, pages 205–235. Springer, 2015.

Outline

⑥ Acknowledge

⑦ References

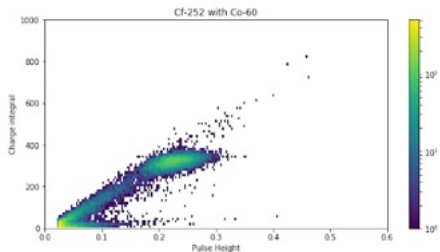
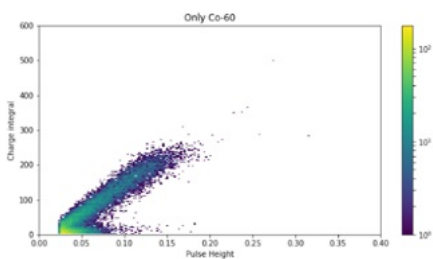
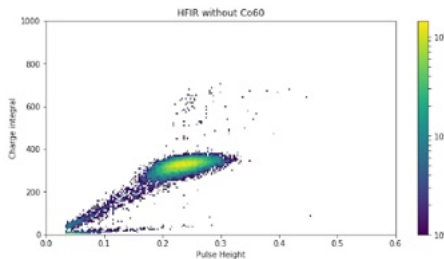
⑧ Appendix

GS20 properties [33]

Properties	GS20
Density (g/cm ³)	2.50
Coefficient of linear expand/°C	9.23×10^{-6}
Light output relative to anthracene*	20-30%
Light yield (photons/absorbed neutron)	~ 6,000
Fast/slow/90% to 10% decay times (ns)	18/57/98
Wavelength of maximum emission (nm)	395
Refractive index at maximum emission	1.55

* Determined by thickness, increasing with decreasing thickness down to $\approx 2\text{ mm}$

GS20 Response to Neutrons and γ -rays Using PMT (Hamamatsu ET60098)

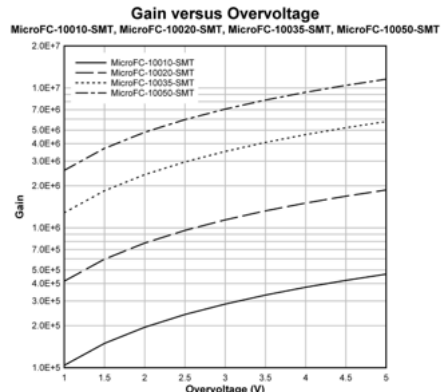
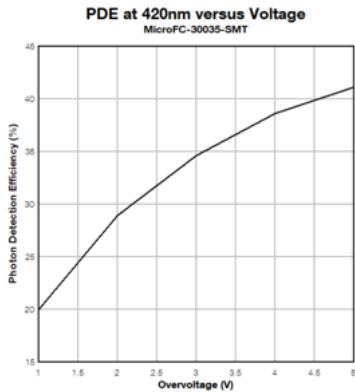


SiPM Characteristics (SensL SiPM)

Characteristics of SensL SiPM (ArrayC-10035064P-BGA). Values are quoted for 1 mm sensor size, microcell size of 35 μm and overvoltage of 2.5 V [20].

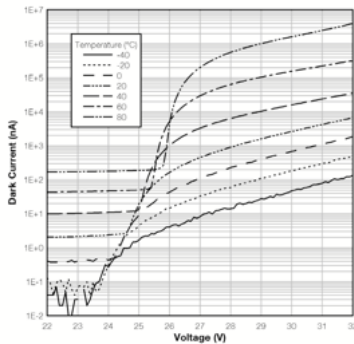
Properties	Nominal values
Breakdown voltage, V_{br} (V)	24.2 - 24.7
O vervoltage, ΔV (V)	1.0 - 5.0
Spectral range, λ (nm)	300 - 950
Peak wavelength, λ_p (nm)	420
Photon detection efficiency, PDE (%)	31
Dark current ($n\text{A}$)	15
Dark count rate, DCR (kHz)	30
Microcell recharge time constant (ns)	82
Crosstalk (%)	7
Afterpulsing (%)	0.2

SiPM Characteristics (SensL SiPM)

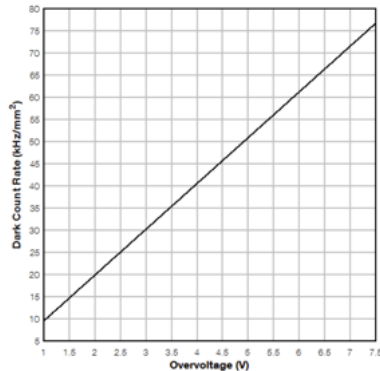


SiPM Characteristics (SensL SiPM)

Dark Current versus Voltage and Temperature
MicroFC-60035-SMT



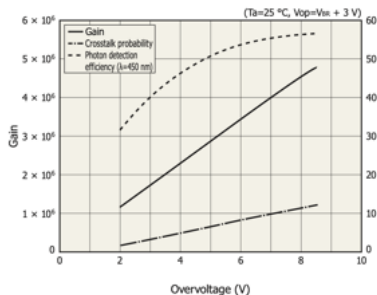
Dark Count Rate versus Overvoltage
MicroFC-30035-SMT (Example Plot)



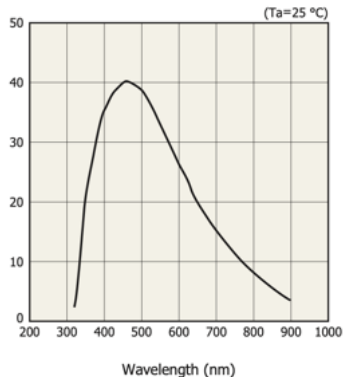
SiPM Characteristics (Hamamatsu SiPM)

Properties	Value
Breakdown voltage, V_{br} (V)	53 ± 5
Overtoltage, ΔV (V)	1.0 - 5.0
Spectral range, λ (nm)	320 - 900
Peak wavelength, λ_p (nm)	450
Photon detection efficiency, PDE (%)	40
Dark count rate, DCR (kHz)	300
Crosstalk (%)	5

SiPM Characteristics (Hamamatsu SiPM)



Photon detection efficiency (%)



Wavelength (nm)

Comparison between SensL ArrayC-10035064P-BGA SiPM (shortened as SensL SiPM) and Hamamatsu S13361-2050AE-08 MPPC array (shortened as Hamamatsu MPPC).

	SensL SiPM	Hamamatsu MPPC
Number of pixels	8×8	8×8
Photosensitive area/channel (mm^2)	1×1	2×2
Number of microcell	504	1584
Microcell size (μm)	35	50
Microcell fill factor (%)	64	74
Array pitch (mm)	2.0	2.2
Dead space between pixels (mm)	1.0	0.2
Breakdown voltage, V_{br} (V)	24.2 - 24.7	53 ± 5
Overtoltage, ΔV (V)	1.0 - 5.0	1.0 - 5.0
Spectral range, λ (nm)	300 - 950	320 - 900
Peak wavelength, λ_p (nm)	420	450
Photon detection efficiency, PDE (%)	31	40
Dark count rate, DCR (kHz)	30	300
Crosstalk (%)	7	5
Afterpulsing (%)	0.2	-

Comparisons between the first prototype and the second prototype.

Changes	First prototype	Second prototype
Detector area (mm^2)	16×16	35.6×35.6
Number of channels	8×8	16×16
Active area per pixel (mm^2)	1×1	1.8×1.8
Dead space per pixel (mm^2)	1×1	0.4×0.4
Pixel pitch (mm)	2.0	2.2
Dimension of a scintillator (mm^3)	$2.0 \times 2.0 \times 2.0$	$1.8 \times 1.8 \times 2.0$
Presence of substrate glass	None	Quartz
Scintillator array manufacturer	ORNL	ORNL + IRD Glass
Reflective coating	BC-620 (TiO_2)	Avian-B ($BaSO_4$)
Reflectance (%)	90	97
Thickness of reflective coating (mm)	0.1-0.2	0.4
SiPM model	SensL ArrayC-10035064P-BGA SiPM	Hamamatsu MPPC array S13361-2050AE-08
Photosensitive area per pixel (mm)	1.0	2.0
Dead space per pixel (mm)	1.0	0.2
Pixel pitch (mm)	2.0	2.2
Photon detection efficiency (%)	31	40
Dark count rate (kHz)	30	300
Bias voltage + Overvoltage (V)	27.5	57
SiPM readout system	CROC board	PETsys Readout System
Signal processing	Pulse height discrimination + Time-over-threshold	Charge integration
Time-of-flight	not supported	supported
ASIC	-	TOFPETv2